ACS APPLIED MATERIALS & INTERFACES

www.acsami.org

Research Article

Single Polylactic Acid Nanowire for Highly Sensitive and Multifunctional Optical Biosensing

Weina Zhang, Pu Liu, Guowei Yang, and Hongxiang Lei*

Cite This: *ACS Appl. Mater. Interfaces* 2021, 13, 27983–27990

Read Online

ACCESS | Metrics & More | Article Recommendations | Supporting Information

ABSTRACT: Nanowire-based optical biosensors with high sensitivity are highly desired for the detection of biological microenvironments and analysis of cellular processes. However, the current nanowire biosensors are mostly fabricated with metal and semiconductor materials, which are not suitable for long-term use in biological environments due to their incompatible and nondegradable properties. Biosensors based on biofriendly materials (e.g., spider silk) often do not have high enough sensitivity due to high losses or micron sizes. Here, polylactic acid (PLA), a polymer with high optical transparency, good biocompatibility, biodegradability, and flexibility, is used to fabricate nanowires using a directly drawing method for the first time. Because of the strong evanescent wave and abundant carboxyl groups on the surface of nanowires, an ultralow concentration sensing of cytochrome *c* is achieved with a limit of detection of 1.38×10^{-17} M, which is much lower than other detection results using semiconductor/metal-based nanosensors (10^{-6} to 10^{-12} M). On this basis, a label-free and real-time monitoring of cell apoptosis is realized. In addition, by doping quantum dots, the functionalized PLA nanowires can also sense a change in pH. These results are suggestive of the potential for PLA nanowires applied in multifunctional biosensing and biodetection, pushing forward the photomedicine field.

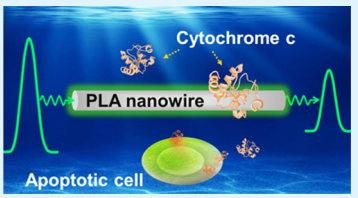

KEYWORDS: *polylactic acid, nanowire, cytochrome c, cell apoptosis, biosensor*

INTRODUCTION

Biological processes in cells and even on a molecular scale, such as cell apoptosis and DNA transcription, can release some biological signals, but they are often too weak to detect.[1,2] Hence, a biosensor with a small size and high sensitivity is highly needed. Due to the small size and large surface-to-volume ratio, nanowire biosensors have high sensitivity and fast responses. Further combining with the advantages of optical detection, such as anti-electromagnetic interference and multiple retrieval signals, nanowire-based optical biosensors have been powerful tools in biosensing and detection.[3−5] For guiding light and sensing simultaneously in biomedical environments, the used nanowires require not only high sensitivity but also great biocompatibility, biodegradability, flexibility, and simple fabrication and modification processes.[6] However, it is currently limited by materials design and fabrication strategies. Until now, the nanowire-based optical waveguides and sensors applied in biomedical fields were made of metallic and semiconductor materials.[7−10] For example, Ag nanowire-coated polymer fiber probe was applied for optoelectronic probing of spinal cord circuits;[7] single-cell endoscopy was fabricated by bonding a SnO_2 nanowire to a silica optical fiber probe;[8] and silicon nanowire arrays were designed and used for C-reactive protein and hepatitis B virus detection.[9,10] The above devices are efficient, but the used materials lack biocompatibility, biodegradability, and flexibility at the same time, which is unfavorable for in-depth applications in biomedical fields. In order to solve this problem, protein materials such as natural silk produced by silkworms and spiders are used to make waveguides and sensors.[11−13] These protein-based fibers have excellent biocompatibility, and they are biodegradable. However, the cost of these protein-based fibers is typically high, and their radial sizes are generally in the order of micrometers, which is not suitable for optical integration and achieving high-sensing sensitivity. Of course, protein-based nanowires with diameters from 150 to 700 nm have been also fabricated by the femtosecond laser direct writing technology.[14] They can guide light and sense biotin, but the propagation loss is about 50−60 dB/mm in the visible wavelength, which is much higher than that for the inorganic material and polymer-based optical waveguides.[15,16] Hence, flexible nanowires which are highly efficient, easily available, low cost, biocompatible, and degradable are highly desired in the biomedical field.

Polylactic acid (PLA) is a synthetic polyester derived from renewable resources such as corn, potato, and beets.[17] Due to its favorable biocompatibility and safe degradation products, PLA has been one of the most important polymers in biomedical use; examples range from tissue engineering, drug

Received: May 1, 2021
Accepted: June 2, 2021
Published: June 10, 2021

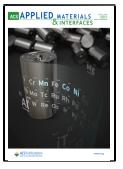

https://doi.org/10.1021/acsami.1c08074
ACS Appl. Mater. Interfaces 2021, 13, 27983−27990

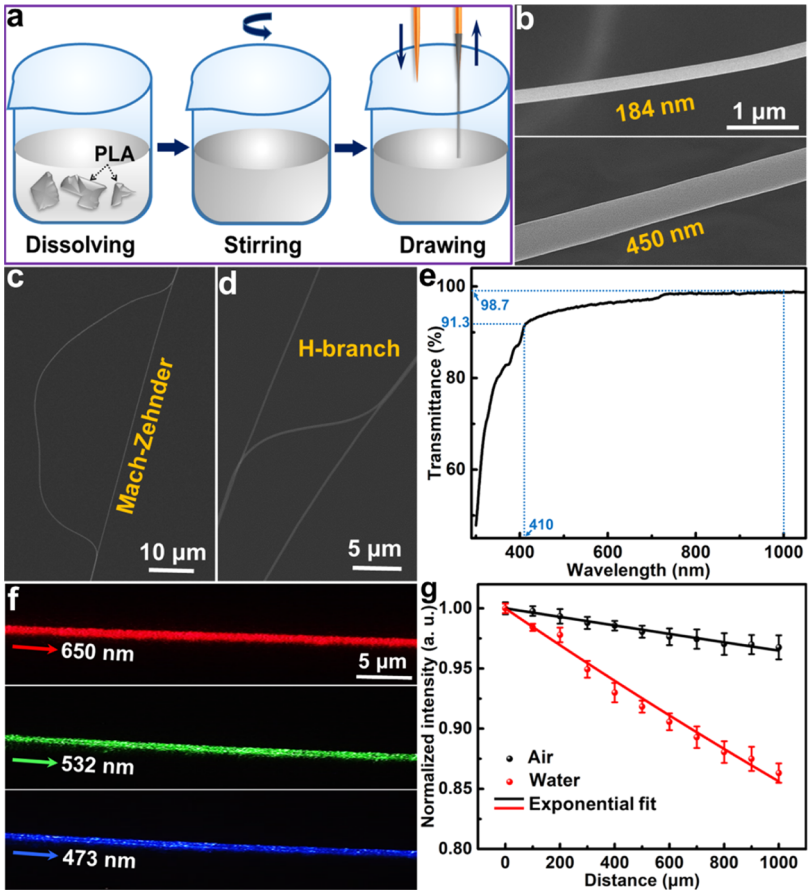

Figure 1. (a) Fabrication process of PLA nanowire. (b–d) SEM images of PLA nanowires and two typical shapes constructed by PLA nanowires. (b) PLA nanowire with a diameter of 184 (upper) and 450 nm (lower). (c) Asymmetric Mach–Zehnder structure. (d) H-branch structure. (e) Transmission spectrum of a 560 nm-diameter PLA nanowire. (f) Dark-field optical microscope images of monochromatic light propagating along the 560 nm-diameter nanowire at wavelengths of 650, 532, and 473 nm. (g) Attenuation of 650 nm light transmitted through the PLA nanowire in air (black dots) and water (red dots) and their exponential fitted curves.

delivery, implants to therapy, and diagnostics.[18−23] Besides, their low extinction and high refractive indices (~1.46) make them suited for optical waveguide devices. To date, PLA-based optical waveguides have been fabricated for deep-tissue photomedicine by melt pressing, solvent casting, ultraviolet-induced crosslinking, and then high-precision laser cutting techniques,[24] for optical neural interfaces and conceptual photodynamic therapy by a thermal drawing process,[25,26] for light delivery into tissue by press-molding method,[27] and by an extrusion-based printing technology.[28] The sizes of the above waveguides are on the order of hundreds of microns. To our knowledge, single PLA nanowire-based optical waveguides and biosensors have not yet been reported. Compared with microfibers, nanowires cause less damage to the biological samples and have stronger light confinement, more sensitivity for environment variation, and higher integration. Therefore, the PLA nanowire-based optical waveguide devices are of great research significance.

Therefore, in this work, single PLA nanowires with various diameters (≥184 nm) are readily fabricated by a directly drawing method. The light input and detection are realized through an evanescent coupling method by two tapered fibers. The excellent light propagation performance of the PLA nanowire waveguides is demonstrated in both air and water environments. Then, utilizing the sensitivity of the evanescent wave to the environment, ultralow concentration sensing of cytochrome *c* (cyt *c*) and real-time monitoring of the apoptosis process of yeast cells by PLA nanowire are achieved. In addition, functionalized PLA nanowire-doped quantum dots (QDs) (CdSe/ZnS) are readily fabricated and applied in pH sensing. The results show that PLA nanowire waveguide devices have broad application prospects in the biomedical and sensing fields.

RESULTS AND DISCUSSION

Figure 1a shows the fabrication process of PLA nanowire. First, as a solvent, an appropriate amount of dichloromethane was mixed with block PLA materials (purchased from Guangzhou Trenrde Tech. Co., Ltd.). Next, the mixture was stirred under a magnetic stirrer to form a homogeneous PLA solution. Finally, a tapered fiber was inserted into the PLA solution and then pulled out quickly. With the rapid evaporation of dichloromethane, PLA nanowire can be drawn from the solution which sticks to the end of the tapered fiber (see the Experimental Section for details) with good homogeneity and continuity (Figure S1 in the Supporting Information). By controlling the concentration of the PLA solution and the drawing speed, size-controlled PLA nanowires can be obtained (Figure S2 in the Supporting Information). As examples, Figure 1b shows the scanning electron microscopy (SEM) images of PLA nanowires with diameters of 184 (upper) and 450 nm (lower). It can be seen that the PLA nanowires exhibit good uniformity

https://doi.org/10.1021/acsami.1c08074
ACS Appl. Mater. Interfaces 2021, 13, 27983−27990

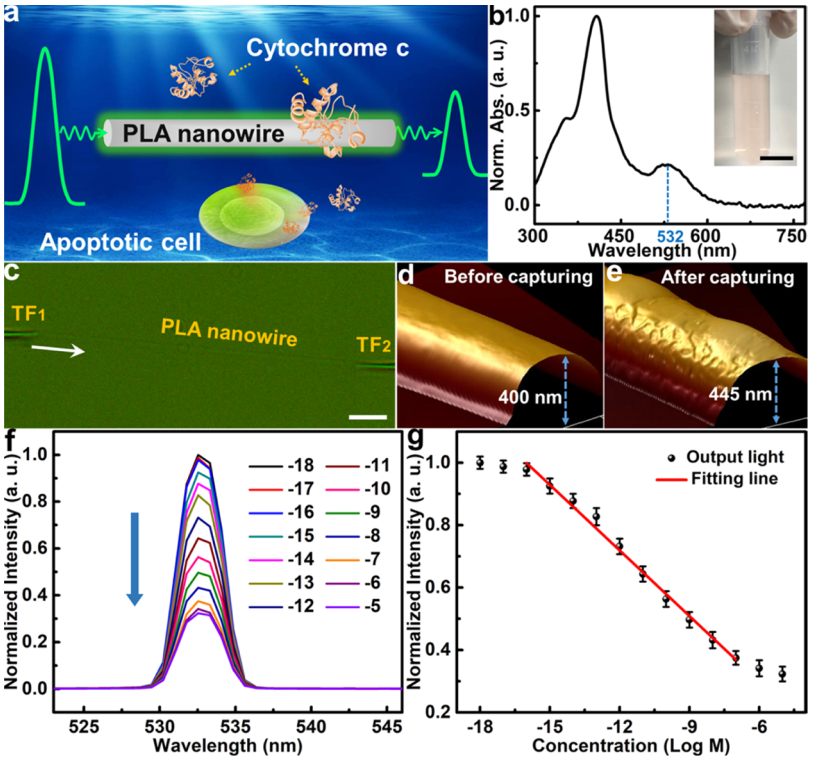

Figure 2. (a) Schematic of cyt *c* detection with a single PLA nanowire. (b) Absorption spectrum of cyt *c*. Inset is an optical image of cyt *c* water solution, and the scale bar is 1 cm. (c) Optical microscope image of PLA-nanowire-based biosensor. Here, the biosensor is a 400 nm-diameter PLA nanowire with a sensing length of 100 μm. The scale bar is 10 μm. (d,e) 3D AFM images of the PLA nanowire surface before (d) and after (e) capturing cyt *c*. (f) Output light spectra with cyt *c* concentration changing from 10^{-18} to 10^{-5} M. (g) Concentration-dependent output light intensity. The red line is the linear fitting line for the concentration from 10^{-16} to 10^{-7} M.

and sidewall smoothness, indicating that there is no obvious defect on the surface of the nanowire, which is contributed to low-loss light transmission. Then, a transmission electron microscopy (TEM) image of a 120 nm-diameter PLA nanowire with electron diffraction pattern was captured to investigate the inner part of the PLA nanowire (see Figure S3 in the Supporting Information). It shows that the PLA nanowires are solid cylinders with a uniform inner part, which has no contribution to the optical loss of light propagation. By using a high-precision micro-manipulator to cut, position, twist, and pull the nanowires under an optical microscope, the PLA nanowires can be easily and repeatedly designed into a variety of shapes. Figure 1c,d shows two typical shapes of Mach−Zehnder and H-branch structures, respectively, indicating the great flexibility of the PLA nanowires. To demonstrate this more deeply, the structures based on PLA nanowires with greater bending degrees were fabricated. The SEM image (Figure S4 in the Supporting Information) shows two flexible rings with bending radii as small as 495 and 256 nm, which is a strong proof of distinguished flexibility. Besides, the PLA nanowire (560 nm-diameter as an example) displays high optical transparency (>91%) for light with a wavelength ranging from 410 to 1000 nm and the highest transmittance is even 98.7% at 1000 nm (Figure 1e). The characteristics of smooth surface, good flexibility, and high transmittance of PLA nanowires make them very suitable for low-loss optical transmission devices.

To evaluate light-guiding properties of PLA nanowires in depth, light was guided into the nanowire through evanescent wave coupling.[29] Figure 1f shows the dark-field optical microscope images of monochromatic light propagating along the 560 nm-diameter PLA nanowire at wavelengths of 650 (upper), 532 (middle), and 473 nm (lower). The lights can transmit along the waveguide for a long distance with a slight change in light intensity. Using a cutback method[29] the optical propagation loss of the PLA nanowire was measured (see Figure S5 in the Supporting Information for details). It is noteworthy that the coupling coefficient between the evanescent wave coupling tapered fibers and the PLA nanowire has no influence on the optical propagation loss measurements. Figure 1g shows the normalized intensity of 650 nm light transmitted through the PLA nanowire in both air (black dots) and water (red dots). The light intensity decreases with the increasing propagation distance, and the date can be well fitted by an exponential equation with $R^2 > 0.99$. Moreover, the light intensity decreases faster in water than in air, indicating that different surface refractive index will affect the optical propagation loss of the PLA nanowires. The optical propagation loss for 650 nm light is calculated as 0.14 and 0.64 dB/mm in air and water, respectively. By the same method, attenuation of 532 and 473 nm light transmitted through the PLA nanowire in both air and water was measured (see Figure S6 in the Supporting Information), and the optical propagation loss for 532 and 473 nm light can be calculated as 0.16 and 0.23 dB/mm in air and 0.72 and 1.35 dB/mm in water, respectively. These results show that PLA nanowires can effectively conduct light propagation in both air and water environment, and the longer light wavelength corresponds to the smaller propagation loss, agreeing with the transmission spectrum of the PLA nanowire in Figure 1e. It is noteworthy that the optical propagation loss of the PLA nanowire is 2

https://doi.org/10.1021/acsami.1c08074
ACS Appl. Mater. Interfaces 2021, 13, 27983−27990

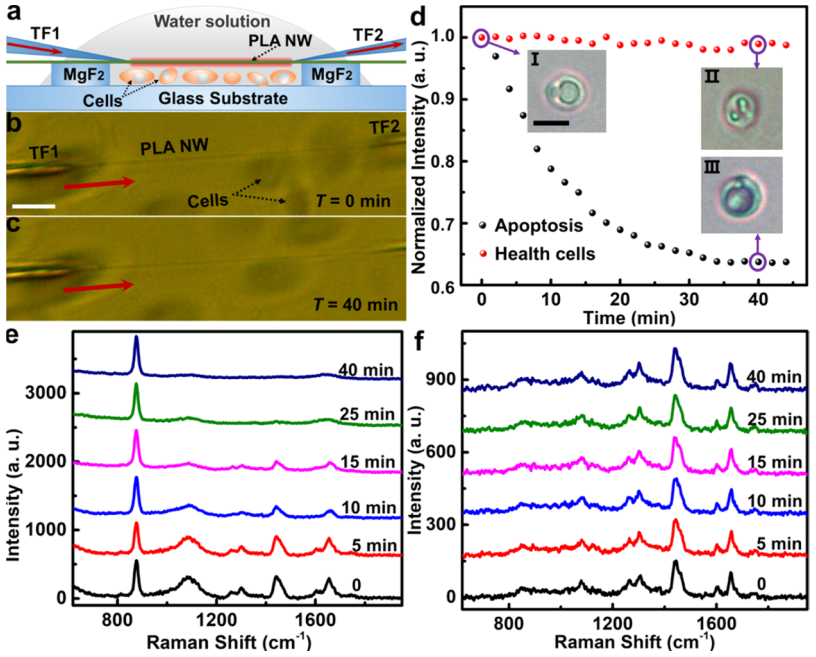

Figure 3. (a–d) Real-time monitoring of biological cell apoptosis by a single PLA nanowire. (a) Schematic of the experiment. The cells used here were yeast cells. (b) Optical microscope image of the biosensor at the time H_2O_2 is just added (T = 0). The scale bar is 15 μm. (c) Optical microscope image of the biosensor at T = 40 min. (d) Time-dependent output light intensity for apoptotic cells (black data, with H_2O_2) and healthy cells (red data, without H_2O_2). Insets are the optical microscope images of the yeast cells stained by trypan blue. The scale bar is 10 μm. (e,f) Raman spectra at a different time for the (e) apoptotic and (f) healthy yeast cell samples.

orders of magnitude smaller than some protein-based nanowires.[14]

When light propagates in the nanowire, a part of it is exposed to the environment and propagates in the form of evanescent waves. These evanescent waves are sensitive to environmental changes. Therefore, using this surface-sensitive effect, nanowires are often used for highly sensitive sensing and detection.[14,30,31] As an important biological indicator, the detection of cyt *c* is of great significance to monitor cell apoptosis and it has gained increasing research attention.[32−35] However, it is currently limited by the sophisticated structure or high limit of detection. Here, an ultralow concentration detection of cyt *c* by a single PLA nanowire was demonstrated, and the corresponding schematic is shown in Figure 2a. In the apoptotic process, the permeability of the cell membrane changes, resulting in a gradual release of cyt *c* from the inside of the cell into the environment. The capture of the cyt *c* on the PLA nanowire surface causes changes in surface roughness, thickness, and refractive index,[35] resulting in the decrease in intensity of emitted light. Therefore, by monitoring the intensity change of the emitted light, the cyt *c* can be detected by a single PLA nanowire. To quantify the detection ability of PLA nanowires, cyt *c* (Sigma, C7752) water solutions with different concentrations were prepared. Figure 2b shows the absorption spectrum of cyt *c* in water solution. As an example, the inset is the optical image of the cyt *c* water solution with a concentration of 1 mg/mL. It can be seen that the cyt *c* has two absorption peaks at 408 and 526 nm. Considering the propagation loss, absorbance of cyt *c*, and suitability for biological samples, 532 nm-wavelength laser with 10 mW power was chosen as the input light source. As an example, a 400 nm-diameter PLA nanowire with a sensing length of 100 μm (i.e., light propagation distance) is used to detect the cyt *c* in water solution. Two ends of the nanowire are supported by two MgF_2 crystals, and the main part of the nanowire is suspended above a channel (~3 mm width). The MgF_2 used here was to achieve a proper refractive index matching and then a better light-guiding performance. As we know, the refractive index of MgF_2 (1.39) is less than those of the glass (1.45) and PLA (1.46), ensuring tight light confinement for the nanowire and little light leakage to the glass substrate. As Figure 2c shows, the incident light was coupled into the PLA nanowire by tapered fiber 1 (TF_1) and the emitted light was detected by a spectrometer via tapered fiber 2 (TF_2). PLA nanowires are weakly acidic and have carboxyl groups on the surface, and thus the cyt *c* in the solution will be attached to the surface of the nanowire through the binding between the amino groups of cyt *c* and carboxyl groups of the nanowire. Figure 2d,e shows the three-dimensional (3D) atomic force microscopy (AFM) images of the nanowire surface before and after capturing cyt *c*, respectively. It can be seen that the surface of the pure PLA nanowire is very smooth, which agrees with the above results in Figure 1. After capturing cyt *c*, the thickness and roughness of the nanowire are obviously observed. Figure 2f,g shows the emitted light spectra and the intensity with the different concentrations of cyt *c* changing from 10^{-18} to 10^{-5} M, respectively. The emitted light intensity decreases with the increasing cyt *c* concentration and the linear range is 10^{-16} to 10^{-7} M with a linearity of 97.1%. The limit of detection (LOD) of this sensor can be calculated as 1.38×10^{-17} M (see "Calculation of the LOD" in the Supporting Information for details). The result is much lower than that obtained previously by an electrochemiluminescence aptasensor (~10^{-12} M),[32] a CdTe optical nanosensor (~10^{-6} M),[33] and a gold-nanotriangle nanosensor (~10^{-9} M),[34] and it is also comparable to that achieved by an optical microfiber aptasensor decorated with silver-nanoparticle-functionalized graphene nanointerface.[35] Obviously, compared with the

https://doi.org/10.1021/acsami.1c08074
ACS Appl. Mater. Interfaces 2021, 13, 27983−27990

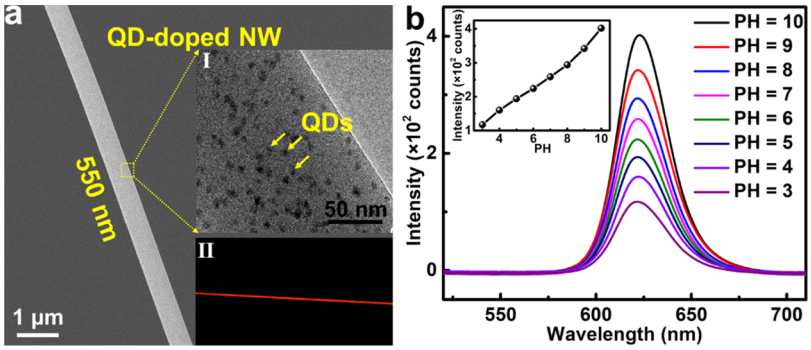

Figure 4. (a) SEM image of a QD-doped PLA nanowire with 550 nm diameter. Inset I is the TEM image of the nanowire. Inset II is the optical microscope image of the nanowire under a 473 nm excitation. (b) PL spectra of the QDs at different pH values. Inset is the pH-dependent PL intensity.

reported methods, our method is more efficient, simple, easy to process, and low cost. This ultralow LOD obtained in this work is mainly attributed to the following reasons. First, the nanoscale size of the PLA nanowire makes the stronger evanescent wave exposed to the environment and its large surface-to-body ratio is also beneficial to the full contact between the sensor and the environment. In addition, the carboxyl groups of the PLA nanowire surface facilitate the capture of cyt *c*, which will cause changes in the surface roughness and thickness of the nanowire and then vary its surface refractive index and affect the output light intensity. Besides, the strong absorption of cyt *c* at 532 nm makes the sensor more sensitive. Under the combined effect of the above factors, an ultralow concentration sensing of cyt *c* is achieved by the single PLA nanowire, which is more beneficial to monitor or find the initial stage of cell apoptosis.

In addition to the highly sensitive sensing, the PLA nanowires also have good biocompatibility and biodegradability[25,36] (see Figures S7 and S8 in the Supporting Information for details). Based on the above characteristics, the PLA nanowire was further used for real-time monitoring of biological cell apoptosis. Figure 3a shows the schematic diagram of the experiment. The used cells were yeast cells because they are rich in cyt *c*. The cells were dispersed in a water solution with a cell concentration of 1.96×10^3 cells/mm^2 (Figure S9 in the Supporting Information). H_2O_2 with a concentration of 0.8 wt % was used as the inducer of apoptosis. Taking the above 400 nm-diameter PLA nanowire with a sensing length of 100 μm as an example, Figure 3b shows the optical microscope image of the PLA-nanowire-based biosensor in the cell solution at $T = 0$, that is, the time H_2O_2 is just added. The yeast cells sunk near the substrate. As immotile and symmetrically shaped cells, the only movement of the sunk live yeast cells was the Brownian movement. Hence, the movement amplitude of the yeast cells was small during the sensing process. The nanowire sensor is suspended above a channel, with ~3 mm width and ~1 mm height. The far enough distance between the nanowire sensor and the yeast cell also ensures that the sensing process will not be affected by the movement of the yeast cell. The input light was a 532 nm laser with an optical power of 10 mW, which caused no damage to the cells.[37,38] The direction of the red arrow represents the direction of light propagation. After 40 min (Figure 3c), the relative positions between the TFs and the nanowire have no change, proving the good stability of the sensing structure. Figure 3d (black data) shows the time-dependent output light intensity. It can be seen that the output light intensity decreases with the increasing time, representing the increase of environmental refractive index (RI) caused by the increase of cyt *c* concentration. After 34 min, the light intensity decreases 36% and then remains stable, which means that almost all cells in the solution have been in an apoptotic state. For comparison, a healthy cell solution (i.e., no H_2O_2 added in it) with the same cell concentration was prepared and monitored in the same way. The time-dependent output light intensity for the healthy cell solution is shown in Figure 3d (red data). With the increase in time, the light intensity fluctuates slightly, meaning that the yeast cells without H_2O_2 can maintain good activity within 40 min. Additionally, it should be pointed out that there is a sophisticated physical and chemical microenvironment in the local apoptotic area, especially the variation of pH value;[39] however, our experiment has demonstrated that the variation of pH value could not interfere with the detection by the optical sensor (see Figure S10 in the Supporting Information). Besides, the specificity of detection for cyt *c* in our work was ensured by selecting an input light with an appropriate wavelength (see Figure S11 in the Supporting Information for details).

In order to further verify the experimental results, trypan blue tests were also conducted for the yeast cell samples with/without H_2O_2. At $T = 0$, both groups of cells could not be stained, as shown in inset I of Figure 3d, meaning that the cells have a good activity at the beginning. After 40 mins, the yeast cells without H_2O_2 were still not stained (inset II of Figure 3d). At the same time, the yeast cell with H_2O_2 was stained blue (inset III of Figure 3d), representing the death of the yeast cell. This result is consistent with that monitored by the single PLA-nanowire-based biosensor. Nevertheless, the comparison between inset I and III also indicates that there is no great difference in the morphology of healthy and dead cells, which may be due to the presence of the cell wall. Moreover, due to the small sizes of yeast cells (4−10 μm), the staining results are not particularly obvious. Hence, Raman spectroscopy of the yeast cells with/without H_2O_2 at different times was further carried out to monitor the apoptosis process of the cells, as shown in Figure 3e,f, respectively. In Figure 3e, there are six Raman peaks with centers at 876, 1081, 1259, 1301, 1440, and 1654 cm^{-1}, in which the 876 cm^{-1} peak is resulting from the presence of H_2O_2 and the others belong to the yeast cell. For the yeast cells with H_2O_2, the intensities of all of the Raman peaks decrease with the increasing time, meaning the increasing of cell apoptosis degree. For the yeast cells without H_2O_2, the Raman peaks were always obviously during 40 min. The above results show that H_2O_2 can cause

https://doi.org/10.1021/acsami.1c08074
ACS Appl. Mater. Interfaces 2021, 13, 27983−27990

the apoptosis of yeast cells, which can be monitored in real-time by a single PLA nanowire.

Additionally, PLA nanowires can be easily functionalized due to the polymer characteristics. By doping different materials, PLA nanowires can be applied in multiple fields. As an example, a common QD, CdSe/ZnS, was doped in PLA nanowires and then a high-resolution pH-sensing experiment was performed. More specifically, the CdSe/ZnS QDs used here were first modified by carboxyl groups and dispersed in acetone solution, which were purchased from Wuhan Jiayuan Quantum Dots Co., Ltd. Then, the QDs were mixed in PLA solution with a mass ratio of QDs to PLA = 1:3000. Finally, the QD-doped nanowires were fabricated by a directly drawing method. Figure 4a shows the SEM image of a QD-doped PLA nanowire with a diameter of 550 nm, and inset I is the TEM image of the nanowire. The QDs were evenly distributed in the nanowire. Inset II is the optical microscope image of the nanowire under an excitation of 473 nm light. The uniform red light emitted along the nanowire indicates again that the QDs are successfully and uniformly doped in the nanowire. Due to the pH sensitivity of the QDs,[40,41] the QD-doped PLA nanowire with a sensing length of 100 μm was further used in pH sensing. The pH value of the water solution was varied from 3 to 10 by using boric acid and sodium hydroxide as buffers. A 473 nm incident light with an optical power of 10 mW was coupled into the nanowire by a tapered fiber to excite QD emission. After 100 μm propagation length, the output light spectra were measured by a spectrograph through another tapered fiber. Figure 4b shows the output light spectra from 525 to 710 nm, that is, the photoluminescence (PL) spectra of the QDs, at different pH solutions. The inset is the pH-dependent PL intensity. Under an excitation of 473 nm light, a 625 nm emission can be excited and measured. The QD-doped nanowire is highly sensitive to pH. As pH increases, the output fluorescence intensity increases monotonically. This can be explained as follows. With the increasing pH, the ionization of the carboxyl groups on the surface of QDs increases, thereby a negatively charged shell on the surface of the QDs is formed, which can increase the confinement of carriers and then lead to a higher quantum yield and a stronger fluorescence intensity.[41] In addition, based on the pH-dependent output light intensity, the resolution of the nanowire-based pH sensor can be calculated as 1.46×10^{-3} to 3.24×10^{-3} RIU.[42] Compared to other QD-based pH sensors, the QD-doped nanowires are easy to recycle and reused. Moreover, doping QDs in nanowires can effectively solve the problem of sample contamination due to the diffusion and leakage of the QDs.[41,43]

CONCLUSIONS

In summary, a novel optical waveguide and biosensor based on a single PLA nanowire were fabricated through a directly drawing method. As a waveguide device, PLA nanowires have outstanding optical performance such as high flexibility, high plasticity, highly transmittance (>91% for visible and near-infrared light), and low propagation loss (0.14 and 0.64 dB/mm for 650 nm light in air and water, respectively). Meanwhile, they have great biocompatibility and biodegradability, which is favorable for their in-depth applications in biomedical fields. Utilizing the surface-sensitive effect, the PLA nanowires can be used as biosensors and ultralow concentration sensing of cyt *c* is achieved by a single PLA nanowire with LOD of 1.38×10^{-17} M. Combining the excellent biocompatibility and sensing properties, the PLA nanowire was further used to realize label-free and real-time monitoring of biological cell apoptosis. Furthermore, as a polymer nanowire, the PLA nanowire is easy to be modified. Through doping pH-sensitive QDs, a pH sensor based on a QD-doped single PLA nanowire was fabricated and the highest pH resolution of 1.46×10^{-3} RIU was obtained. Therefore, this work represents a step forward in the development of PLA nanowire-based all-photonic integrated devices applied in biophotonics, biomedicine, and so forth.

EXPERIMENTAL SECTION

Fabrication of the PLA Nanowire. First, 4 g of solid PLA materials and 30 mL of dichloromethane were mixed and kept under magnetic stirring at 25 °C for 5 h to form a PLA solution with appropriate viscosity for drawing. Then, a silica optical fiber taper with a tip diameter of 4 μm was immersed into the sample solution. As soon as the taper was pulled out at a speed of ~1 m s^{-1}, the viscous solution on the tip was extended into a long wire because of the rapid evaporation of dichloromethane. As a result, a PLA nanowire was obtained. By changing the concentration of the PLA solution and the drawing speed, the diameter of the PLA nanowires can be controlled. To ensure the homogeneity and continuity of the nanowires, an appropriate concentration of PLA solution (0.1−0.2 g/mL in our work), a uniform drawing speed, and a stable experimental environment (temperature: 25 °C; humidity: 60%; no obvious airflow) were needed.

Apparatus and Measurements. SEM and TEM (Zeiss Gemini Ultra-55; TEM, JEM-200CX) were used to observe the surface morphologies of the PLA nanowires. The transmission spectrum of PLA nanowires is measured by a microspectrophotometer (CRAIC 20, 20/20PV). The sources of light (650, 532, and 473 nm) coupled into the nanowire are semiconductor monochromatic lasers, and the output light spectra were collected by a spectrometer (Ocean Optics, QE65 Pro) with an integral time of 0.1 s. Raman spectra are measured by a Horiba XploRA PLUS Confocal Raman microscope (Horiba, Kyoto, Japan). A 532 nm-laser with an optical power of 10 mW was used for excitation. The integral time and accumulation number of the Raman spectrum detection were set as 10 and 5 s, respectively, which could be averaged to reduce an error.

ASSOCIATED CONTENT

Supporting Information

The Supporting Information is available free of charge at https://pubs.acs.org/doi/10.1021/acsami.1c08074.

Homogeneity and continuity of the PLA nanowires; relationship of the drawing speed and nanowire size; characterization of the inner part of the PLA nanowires; flexibility of the PLA nanowires; measurement of the optical propagation loss of the PLA nanowires; attenuation of 532 and 473 nm lights transmitted through the PLA nanowire in both air and water; calculation of the LOD; biocompatibility of the PLA nanowires; biodegradability of the PLA nanowires; optical image of the cells dispersed in water solution; impact of the variation in pH on the detection process; and specificity of detection for cyt *c* (PDF)

AUTHOR INFORMATION

Corresponding Author

Hongxiang Lei − *School of Materials Science and Engineering, State Key Laboratory of Optoelectronic Materials and Technologies, Sun Yat-sen University, Guangzhou 510275, China*; Email: leihx@mail.sysu.edu.cn

https://doi.org/10.1021/acsami.1c08074
ACS Appl. Mater. Interfaces 2021, 13, 27983−27990

Authors

Weina Zhang − *School of Materials Science and Engineering, State Key Laboratory of Optoelectronic Materials and Technologies, Sun Yat-sen University, Guangzhou 510275, China;* orcid.org/0000-0002-9752-9079

Pu Liu − *School of Materials Science and Engineering, State Key Laboratory of Optoelectronic Materials and Technologies, Sun Yat-sen University, Guangzhou 510275, China*

Guowei Yang − *School of Materials Science and Engineering, State Key Laboratory of Optoelectronic Materials and Technologies, Sun Yat-sen University, Guangzhou 510275, China*

Complete contact information is available at: https://pubs.acs.org/10.1021/acsami.1c08074

Notes

The authors declare no competing financial interest.

■ ACKNOWLEDGMENTS

This work was supported by the National Natural Science Foundation of China (NSFC) (11974435 and 12004444) and the Natural Science Foundation of Guangdong Province (2018A030313498 and 2016A030313339).

■ REFERENCES

(1) Zhu, D.; Zhang, L.; Ma, W.; Lu, S.; Xing, X. Detection of microRNA in clinical tumor samples by isothermal enzyme-free amplification and label-free graphene oxide-based SYBR Green I fluorescence platform. *Biosens. Bioelectron.* **2015**, *65*, 152−158.

(2) Bhalla, N.; Pan, Y.; Yang, Z.; Payam, A. F. Opportunities and challenges for biosensors and nanoscale analytical tools for pandemics: COVID-19. *ACS Nano* **2020**, *14*, 7783−7807.

(3) Sun, F.; Sun, L.; Zhang, B.; Chen, G.; Wang, H.; Shen, X.; Lu, W. Optical waveguide of buckled CdS nanowires modulated by strain engineering. *ACS Photonics* **2018**, *5*, 746−751.

(4) Kim, S.; Yan, R. Recent Developments in Photonic, Plasmonic and Hybrid Nanowire Waveguides. *J. Mater. Chem. C* **2018**, *6*, 11795−11816.

(5) Sirbuly, D. J.; Law, M.; Pauzauskie, P.; Yan, H.; Maslov, A. V.; Knutsen, K.; Ning, C.-Z.; Saykally, R. J.; Yang, P. Optical Routing and Sensing with Nanowire Assemblies. *Proc. Natl. Acad. Sci. U.S.A.* **2005**, *102*, 7800−7805.

(6) Nazempour, R.; Zhang, Q.; Fu, R.; Sheng, X. Biocompatible and implantable optical fibers and waveguides for biomedicine. *Materials* **2018**, *11*, 1283.

(7) Lu, C.; Park, S.; Richner, T. J.; Derry, A.; Brown, I.; Hou, C.; Rao, S.; Kang, J.; Mortiz, C. T.; Fink, Y.; Anikeeva, P. Flexible and stretchable nanowire-coated fibers for optoelectronic probing of spinal cord circuits. *Sci. Adv.* **2017**, *3*, No. e1600955.

(8) Yan, R.; Park, J.-H.; Choi, Y.; Heo, C.-J.; Yang, S.-M.; Lee, L. P.; Yang, P. Nanowire-based single-cell endoscopy. *Nat. Nanotechnol.* **2012**, *7*, 191−196.

(9) Irrera, A.; Leonardi, A. A.; Di Franco, C.; Lo Faro, M. J.; Palazzo, G.; D'Andrea, C.; Manoli, K.; Franzò, G.; Musumeci, P.; Fazio, B.; Torsi, L.; Priolo, F. New generation of ultrasensitive label-free optical Si nanowire-based biosensors. *ACS Photonics* **2018**, *5*, 471−479.

(10) Leonardi, A. A.; Lo Faro, M. J.; Petralia, S.; Fazio, B.; Musumeci, P.; Conoci, S.; Irrera, A.; Priolo, F. Ultrasensitive label-and PCR-free genome detection based on cooperative hybridization of silicon nanowires optical biosensors. *ACS Sens.* **2018**, *3*, 1690−1697.

(11) Parker, S. T.; Domachuk, P.; Amsden, J.; Bressner, J.; Lewis, J. A.; Kaplan, D. L.; Omenetto, F. G. Biocompatible silk printed optical waveguides. *Adv. Mater.* **2009**, *21*, 2411−2415.

(12) Qiao, X.; Qian, Z.; Li, J.; Sun, H.; Han, Y.; Xia, X.; Zhou, J.; Wang, C.; Wang, Y.; Wang, C. Synthetic engineering of spider silk fiber as implantable optical waveguides for low-loss light guiding. *ACS Appl. Mater. Interfaces* **2017**, *9*, 14665−14676.

(13) Tansil, N. C.; Li, Y.; Teng, C. P.; Zhang, S.; Win, K. Y.; Chen, X.; Liu, X. Y.; Han, M.-Y. Intrinsically colored and luminescent silk. *Adv. Mater.* **2011**, *23*, 1463−1466.

(14) Sun, Y.-L.; Sun, S.-M.; Wang, P.; Dong, W.-F.; Zhang, L.; Xu, B.-B.; Chen, Q.-D.; Tong, L.-M.; Sun, H.-B. Customization of protein single nanowires for optical biosensing. *Small* **2015**, *11*, 2869−2876.

(15) Eaton, S.; Fu, A.; Wong, A. B.; Ning, C. Z.; Yang, P. D. Semiconductor nanowire lasers. *Nat. Rev. Mater.* **2016**, *1*, 16028.

(16) Xia, H.; Chen, T.; Hu, C.; Xie, K. Recent advances of the polymer micro/nanofiber fluorescence waveguide. *Polymers* **2018**, *10*, 1086.

(17) Singhvi, M. S.; Zinjarde, S. S.; Gokhale, D. V. Polylactic acid: synthesis and biomedical applications. *J. Appl. Microbiol.* **2019**, *127*, 1612−1626.

(18) Saini, P.; Arora, M.; Kumar, M. N. V. R. Poly(lactic acid) blends in biomedical applications. *Adv. Drug Delivery Rev.* **2016**, *107*, 47−59.

(19) da Silva, D.; Kaduri, M.; Poley, M.; Adir, O.; Krinsky, N.; Shainsky-Roitman, J.; Schroeder, A. Biocompatibility, biodegradation and excretion of polylactic acid (PLA) in medical implants and theranostic systems. *Chem. Eng. J.* **2018**, *340*, 9−14.

(20) Zhang, S.; Ma, B.; Liu, F.; Duan, J.; Wang, S.; Qiu, J.; Li, D.; Sang, Y.; Liu, C.; Liu, D.; Liu, H. Polylactic acid nanopillar array-driven osteogenic differentiation of human adipose-derived stem cells determined by pillar diameter. *Nano Lett.* **2018**, *18*, 2243−2253.

(21) Tyler, B.; Gullotti, D.; Mangraviti, A.; Utsuki, T.; Brem, H. Polylactic acid (PLA) controlled delivery carriers for biomedical applications. *Adv. Drug Delivery Rev.* **2016**, *107*, 163−175.

(22) Valente, T. A. M.; Silva, D. M.; Gomes, P. S.; Fernandes, M. H.; Santos, J. D.; Sencadas, V. Effect of sterilization methods on electrospun Poly(lactic acid) (PLA) fiber alignment for biomedical applications. *ACS Appl. Mater. Interfaces* **2016**, *8*, 3241−3249.

(23) Xu, T.; Yang, H.; Yang, D.; Yu, Z.-Z. Polylactic acid nanofiber scaffold decorated with chitosan islandlike topography for bone tissue engineering. *ACS Appl. Mater. Interfaces* **2017**, *9*, 21094−21104.

(24) Nizamoglu, S.; Gather, M. C.; Humar, M.; Choi, M.; Kim, S.; Kim, K. S.; Hahn, S. K.; Scarcelli, G.; Randolph, M.; Redmond, R. W.; Yun, S. H. Bioabsorbable polymer optical waveguides for deep-tissue photomedicine. *Nat. Commun.* **2016**, *7*, 10374.

(25) Fu, R.; Luo, W.; Nazempour, R.; Tan, D.; Ding, H.; Zhang, K.; Yin, L.; Guan, J.; Sheng, X. Implantable and biodegradable poly(L-lactic acid) fibers for optical neural interfaces. *Adv. Opt. Mater.* **2018**, *6*, 1700941.

(26) Gierej, A.; Berghmans, F.; Vagenende, M.; Filipkowski, A.; Siwicki, B.; Buczynski, R.; Thienpont, H.; Van Vlierberghe, S.; Geernaert, T.; Dubruel, P. Poly (D, L-lactic acid) (PDLLA) biodegradable and biocompatible polymer optical fiber. *J. Lightwave Technol.* **2019**, *37*, 1916−1923.

(27) Kim, M.; An, J.; Kim, K. S.; Choi, M.; Humar, M.; Kwok, S. J. J.; Dai, T.; Yun, S. H. Optical lens-microneedle array for percutaneous light delivery. *Biomed. Opt. Express* **2016**, *7*, 4220−4227.

(28) Feng, J.; Jiang, Q.; Rogin, P.; de Oliveira, P. W.; del Campo, A. Printed soft optical waveguides of PLA copolymers for guiding light into tissue. *ACS Appl. Mater. Interfaces* **2020**, *12*, 20287−20294.

(29) Gu, F.; Zhang, L.; Yin, X.; Tong, L. Polymer single-nanowire optical sensors. *Nano Lett.* **2008**, *8*, 2757−2761.

(30) Wang, Y.; Gao, B.; Zhang, K.; Yuan, K.; Wan, Y.; Xie, Z.; Xu, X.; Zhang, H.; Song, Q.; Yao, L.; Fang, X.; Li, Y.; Xu, W.; Zhang, J.; Dai, L. Refractive index sensor based on leaky resonant scattering of single semiconductor nanowire. *ACS Photonics* **2017**, *4*, 688−694.

(31) Jiao, L.; Zhong, N.; Zhao, X.; Ma, S.; Fu, X.; Dong, D. Recent advances in fiber-optic evanescent wave sensors for monitoring organic and inorganic pollutants in water. *TrAC, Trends Anal. Chem.* **2020**, *127*, 115892.

(32) Karimi Pur, M. R.; Hosseini, M.; Faridbod, F.; Ganjali, M. R.; Hosseinkhani, S. Early detection of cell apoptosis by a cytochrome C

label-Free electrochemiluminescence aptasensor. *Sens. Actuators, B* **2018**, *257*, 87−95.
(33) Amin, R. M.; Elfeky, S. A.; Verwanger, T.; Krammer, B. Fluorescence-based CdTe nanosensor for sensitive detection of cytochrome C. *Biosens. Bioelectron.* **2017**, *98*, 415−420.
(34) Zhang, J.; Ma, X.; Wang, Z. Surface-enhanced Raman scattering-fluorescence dual-mode nanosensors for quantitative detection of cytochrome c in living cells. *Anal. Chem.* **2019**, *91*, 6600−6607.
(35) Li, H.; Huang, Y.; Chen, C.; Xiao, A.; Hou, G.; Huang, Y.; Feng, X.; Guan, B.-O. Real-time cellular cytochrome c monitoring through an optical microfiber enabled by a silver-decorated graphene nanointerface. *Adv. Sci.* **2018**, *5*, 1701074.
(36) Lyu, S.; Untereker, D. Degradability of polymers for implantable biomedical devices. *Int. J. Mol. Sci.* **2009**, *10*, 4033−4065.
(37) Zou, X.; Zheng, Q.; Wu, D.; Lei, H. Controllable cellular micromotors based on optical tweezers. *Adv. Funct. Mater.* **2020**, *30*, 2002081.
(38) Xin, H.; Li, Y.; Liu, Y. C.; Zhang, Y.; Xiao, Y. F.; Li, B. Optical forces: from fundamental to biological applications. *Adv. Mater.* **2020**, *32*, 2001994.
(39) Xu, M.; Ma, X.; Wei, T.; Lu, Z.-X.; Ren, B. In situ imaging of live-cell extracellular pH during cell apoptosis with surface-enhanced Raman spectroscopy. *Anal. Chem.* **2018**, *90*, 13922−13928.
(40) Maule, C.; Gonçalves, H.; Mendonça, C.; Sampaio, P.; Esteves da Silva, J. C. G.; Jorge, P. Wavelength encoded analytical imaging and fiber optic sensing with pH sensitive CdTe quantum dots. *Talanta* **2010**, *80*, 1932−1938.
(41) Chen, X.; Sun, X.; Xu, W.; Pan, G.; Zhou, D.; Zhu, J.; Wang, H.; Bai, X.; Dong, B.; Song, H. Ratiometric photoluminescence sensing based on Ti3C2 MXene quantum dots as an intracellular pH sensor. *Nanoscale* **2018**, *10*, 1111−1118.
(42) Mollah, M. A.; Razzak, S. M. A.; Paul, A. K.; Hasan, M. R. Microstructure optical fiber based plasmonic refractive index sensor. *Sens. Biosensing Res.* **2019**, *24*, 100286.
(43) Yang, P.; Zhu, Z.; Zhang, T.; Zhang, W.; Chen, W.; Cao, Y.; Chen, M.; Zhou, X. Orange-emissive carbon quantum dots: toward application in wound pH monitoring based on colorimetric and fluorescent changing. *Small* **2019**, *15*, 1902823.

https://doi.org/10.1021/acsami.1c08074
ACS Appl. Mater. Interfaces 2021, 13, 27983−27990